Electrical and optical characterization of $Ag_2V_4O_{11}$ and $Ag_4V_2O_6F_2$

M. I. Bertoni · N. J. Kidner · T. O. Mason · T. A. Albrecht · E. M. Sorensen · K. R. Poeppelmeier

Abstract The two silver vanadium oxide phases—$Ag_2V_4O_{11}$ and $Ag_4V_2O_6F_2$—were prepared by hydrothermal synthesis. The electrical conductivity of both silver vanadate powders was determined by the powder-solution-composite (PSC) method. The conductivities obtained were 0.0085 ± 0.0005 and 0.0005 ± 0.00015 S/cm for the $Ag_2V_4O_{11}$ and $Ag_4V_2O_6F_2$, respectively, the first such report for the $Ag_4V_2O_6F_2$ phase. The optical gap and the transmission where studied by diffuse reflectance. Both were larger for $Ag_4V_2O_6F_2$ than $Ag_2V_4O_{11}$, concomitant with a decrease in carrier content.

Keywords Silver vanadium oxide · Vanadium oxide fluoride · Hydrothermal synthesis · Conductivity

1 Introduction

Vanadium oxides have been a subject of study for years and are successfully employed commercially as a cathode material for primary and secondary lithium power sources [1]. $Ag_2V_4O_{11}$ or silver vanadium oxide (SVO), has been well characterized through the years and is the major commercially used cathode in primary (non-rechargeable) lithium batteries [1–4]. High performance, reliability, and the ability to supply a high power pulse while having a long-term stability make them suitable for critical applications such as in implantable cardioverter defibrillators (ICDs). This kind of high energy density battery is used commonly on patients with tachycardia or fibrillation and is required to supply a pulse as high as 35 J and to have the minimum capacitor charging time as possible [2, 4]. ICDs work most efficiently above 3 V and a goal of this industry has been to increase the capacity of the cathode above that voltage, while maintaining its stability. In order to achieve this, Takeuchi et al. suggested that a greater Ag:V molar ratio is necessary [5]. Recently Sorensen et al. reported a new silver vanadium oxide phase with a Ag:V ratio of 2:1, where some oxide ions have been replaced with more electronegative fluoride anions [6]. The new oxyfluoride phase, $Ag_4V_2O_6F_2$, or silver vanadium oxide fluoride (SVOF) is the first reported phase in the Ag_2O-V_2O_5-AgF system. Sorensen et al. showed that the high mole fraction of silver in SVOF indeed improves the gravimetric capacity above 3 V, from 100 mAh/g for SVO to 148 mAh/g for SVOF. However, as previous work suggests this may be to the detriment of the conductivity [5]. Low electronic conductivity may be desirable for solid electrolytes, but not for battery applications. Mixed conductivity (electronic-ionic) is required to preserve the overall charge neutrality during lithium ion transport, where the chemical diffusion coefficient is rate-limited by the slower species. At the microscale, the typical storage device is composed of a percolating network of storage particles and a moderate electronic conductivity is desirable to prevent the impedance of this device from becoming excessive [7]. In the present study, SVO and SVOF powders were prepared using a hydrothermal technique [6]. Owing to the low temperature character of this synthesis and the stability of these compounds at higher temperatures, conventional four-

M. I. Bertoni · N. J. Kidner · T. O. Mason (✉)
Department Materials Science and Engineering,
Northwestern University,
Evanston, IL 60208, USA
e-mail: t-mason@northwestern.edu

T. A. Albrecht · E. M. Sorensen · K. R. Poeppelmeier
Department Chemistry, Northwestern University,
Evanston, IL 60208, USA

point conductivity measurements on sintered specimens were not possible. Instead, the electrical conductivity of these silver vanadium oxides was studied by the powder-solution-composite method (PSC), allowing for the measurements to be performed directly on the ceramic powders [8]. The PSC technique is based on impedance spectroscopy (IS) and effective medium theory; it uses slurries formed by the ceramic powder in question and electrolytic solutions of varying conductivity to establish the true bulk conductivity of the powder. In this article we report the conductivity values for the $Ag_2V_4O_{11}$ and $Ag_4V_2O_6F_2$ phases, for the first time in the case of the SVOF phase. We also report the optical gap of these materials for the first time (estimated from the absorption edge measured by diffuse reflectance).

2 Experimental

2.1 Caution

Hydrofluoric acid is toxic and corrosive and must be handled with extreme care and protective gear. If contact with the liquid or vapor happens, proper treatment should be followed [9–11].

2.2 Synthesis and characterization

Polycrystalline $Ag_2V_4O_{11}$ was made from a reaction of 0.2678 g (1.155×10^{-3} mol) of Ag_2O (99.5%, DFG), 0.4198 g (2.308×10^{-3} mol) of V_2O_5 (99.6%, Alfa-Aesar), and 0.2328 g (6.051×10^{-3} mol) of $HF_{(aq)}$ (48–50% HF by weight, Fisher) in a heat sealed Teflon [fluoro(ethylene–propylene)] pouch [12]. The pouch was placed in a 125 ml, Teflon lined Parr autoclave, backfilled with 42 ml of deionized H_2O. Up to six other pouches of varied compositions were simultaneously placed in the autoclave. The autoclave was heated at 150 °C for 24 h and cooled at a rate of 6 °C/h. The pouches were opened in air and the contents were vacuum-filtered to retrieve $Ag_2V_4O_{11}$ in 98% yield based on V_2O_5.

$Ag_4V_2O_6F_2$ was synthesized by sealing 0.0911 g (5.009×10^{-4} mol) of V_2O_5, 0.4639 g (2.002×10^{-3} mol) of Ag_2O and 0.3036 g (7.433×10^{-3} mol) of $HF_{(aq)}$ solution in a Teflon (fluoroethylenepropylene) pouch. Similar to the synthesis of $Ag_2V_4O_{11}$ the pouch was placed in a 125 ml Teflon-lined Parr autoclave filled with deionized H_2O to 33% of its volume. The autoclave was then heated for 24 h at 150 °C and cooled to room temperature over an additional 24 h. The pouches were opened in air, and the products were recovered by vacuum filtration.

The resulting products were analyzed by powder X-ray diffraction with Ni-filtered Cu Kα radiation (Rigaku XDS

2000, Danvers, MA). Scans were performed between 10 and 80° in 2θ for routine phase analysis and the PXD patterns were subsequently matched to their respective previously reported files using Jade® software [6].

SEM images of the SVO powder were collected on a Hitachi S-3500 scanning electron microscope (SEM), meanwhile images of the SVOF particles were collected with a JSM-7000F field emission SEM in secondary electron mode.

Conductivity measurements were performed using the powder-solution-composite (PSC) method, which was recently developed to measure the conductivity of loose ceramic powders [8]. The technique involves the measurement of the AC impedance response of slurries or "composites" made from packed powders of ceramics of unknown conductivity infiltrated by or suspended in aqueous electrolytes of known conductivity. In a series of experiments, the conductivity of the solution is varied and crossover behavior is seen in AC impedance spectra (and composite conductivity vs. solution conductivity) allowing for the conductivity of the powder specimen to be determined. It should be stressed that the technique registers total conductivity (ionic plus electronic). A full description of the method is given elsewhere [8]. Powder conductivity must be in the range of the solutions employed, e.g., 10^{-4} to 0.5 S/cm for the commonly employed electrolyte, NaCl. In the present experiments, owing to the reactivity of the SVOF phase with aqueous NaCl (producing AgCl), the electrolyte chosen for these measurements was $AgNO_3$. Aqueous solutions of $AgNO_3$ were prepared ranging from 0.002 M (3.1×10^{-4} S/cm) to 0.75 M (0.065 S/cm). Each of the $AgNO_3$ solutions was mixed with 0.04 g of the vanadium oxide powder to form a slurry, which was placed into the measuring device and allowed to settle. The measuring device consists of a polyethylene tube (4.75 mm ID×20 mm) and two stainless steel plugs. The composite slurry was carefully pressed to a powder volume fraction of 0.2–0.3 (at an inner-electrode spacing of ∼2 mm).

A Solartron 1260 Impedance Response Analyzer was employed with Z-60 personal computer software for data collection (Schlumberger, Houston, TX, USA). Alligator clips at the end of coaxial cables were used to make electrical contact to the stainless steel plugs. The excitation voltage was 1 V and the scans were performed from 10 MHz to 1 Hz, with data collected at 10 steps per frequency decade.

Optical data were obtained from diffuse reflectance measurements. The spectra for the specimens were collected on a Cary 500 UV visible-near infrared spectrophotometer (Varian Instruments Inc., Palo Alto, CA) using a diffuse reflectance accessory between 300–800 nm with a lead sulfide detector. This accessory has the ability to collect most reflected radiation, remove any directional preferen-

ces, and present an integrated signal to the detector. The data are measured relative to a baseline given by a polytetrafluoroethylene standard that sets the 100% reflection. The optical gap was estimated from the absorption edge that was determined by the intersection of a line drawn through the sloped portion of the transition region between high and low transmission and the baseline of the low-transmission portion of each spectrum.

3 Results and discussion

Figure 1 shows typical Nyquist plots (-Zimag vs. Zreal) for the 0.02 M AgNO$_3$ solution by itself and with 0.25 volume fraction of SVOF phase, with frequency markers (log$_{10}$ of frequency) as shown. For the case of the plain solution we observe an electrode arc extending to low frequencies (to the right) and the beginning of a single electrolyte arc at high frequencies (to the left, below 450 Ω). The dashed semi-circle represents the electrolyte response, which has been confirmed by time-domain reflectometry measurements in the MHz to GHz range (not shown) (Woo, Kidner, and Mason, unpublished results). The behavior of the plain electrolyte solution can be modeled using an equivalent circuit composed of two parallel resistor–capacitor (RC) elements in series, or (RC)(RC) in the equivalent circuit notation of Boukamp [13]. One RC element represents the solution and the other represents the combined electrodes [8]. Whereas the solution arc, when measured, is not significantly depressed below the real axis, the electrode arc is always depressed, and therefore is more accurately represented as an (RQ) element, where Q represents a constant phase element [13]. This does not, however,

influence the value of electrolyte resistance derived from the intersection of the two arcs along the real impedance axis; this value consistently agrees with the four-point DC resistance of the solution [8].

In the case of the "composite" (0.02 M AgNO$_3$+0.25 volume fraction of SVOF) in Fig. 1 there is just a hint of the start of the electrode arc at low frequencies (on the right). This "cusp" (~880 Ω) agrees nicely with 4-point DC measurements [8]. The "electrolyte" arc (or more appropriately the "composite" arc) is now subdivided into two separate arcs, with a cusp between them at ~280 Ω. There is little or no arc depression in the case of the clearly visible bulk arc. The overall behavior is more fully described in [8], and an equivalent circuit model is provided to simulate the response. The "composite" situation in Fig. 1 involves a regime where the particles are more conductive than the electrolyte in which they are suspended. Owing to a high-impedance interfacial element (electrochemical double-layer/charge transfer resistance) on the surface of the more conductive particles, they behave as if insulated from the "matrix" phase (electrolyte) at low frequencies [8, 14, 15]. Therefore, the bulk/electrolyte or DC resistance shifts to the right (higher resistance) as shown. In effect, the "coated" particles are acting as insulating inclusions. However, displacement currents through the double-layer capacitance short out the high-impedance interfacial element with increasing frequency, rendering the particles more conductive than the matrix phase (electrolyte) at the high frequency cusp resistance, indicated by the arrow in Fig. 1. It should be pointed out that this high frequency cusp resistance is sufficient for the data analyses to follow; equivalent circuit analyses can be performed (as in [8]) but are unnecessary to acquire meaningful PSC results.

What is required for PSC analysis, however, is a knowledge of the particle size/shape of the powders being analyzed and the appropriate mixing laws/effective medium theories to describe their behavior in composites [14–20]. Therefore, SEM images were collected (Figs. 2 and 3) showing the morphology and particle size distribution for the SVO and SVOF phases, respectively. For the case of the SVO, elongated rectangular crystallites ranging from a few microns to 25 μm in length are observed, as well as longer aggregates of smaller primary particles. On the other hand, the SVOF phase presents a more spherical morphology, with large aggregates and clusters ranging from 5 to 70 μm. Owing to the difference in morphology between the two silver vanadates, two different mixing laws are required to describe the composite behavior.

The best fit to the PSC composite data for the SVO particles was given by the model proposed by H. Fricke, in which the Maxwell–Wagner dispersion was extended to a suspension of ellipsoids [21]. If we consider a suspension of ellipsoids (axes $2a \geq 2b \geq 2c$) where the a-axis is much
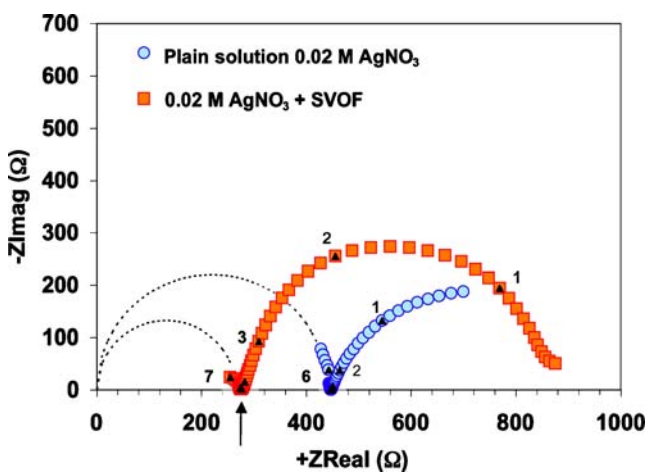
Fig. 1 Experimental Nyquist plot for 0.02 M AgNO$_3$ plain solution (*circles*) and 0.02 M AgNO$_3$ + SVOF composite (*squares*). The composite resistance used for analysis is indicated with an *arrow*. Frequency values representing log ν are labeled (*triangles*)
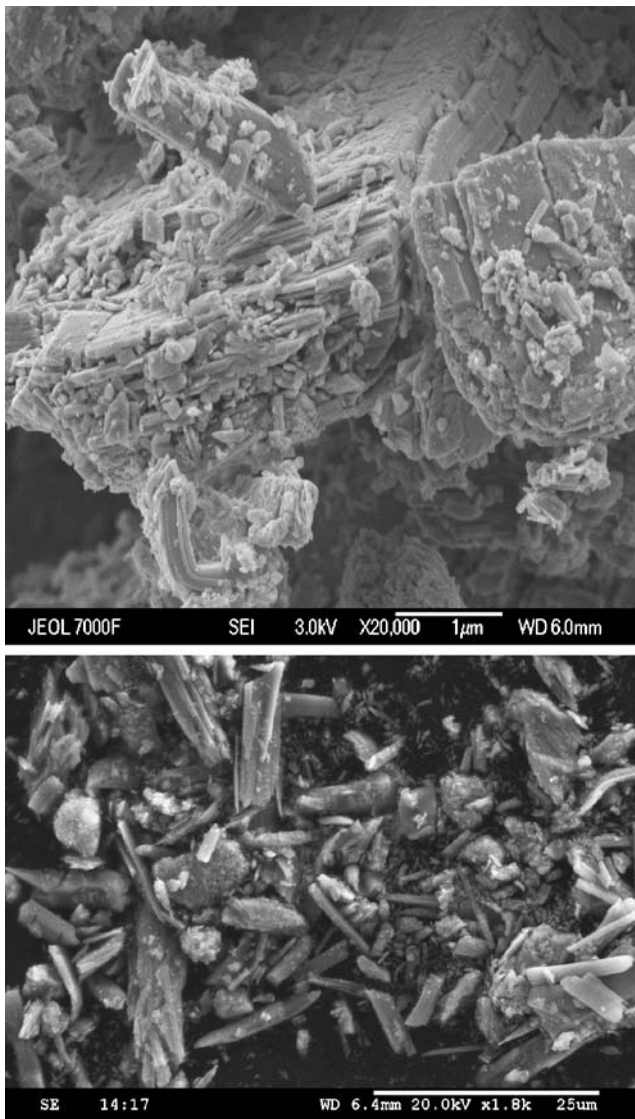
Fig. 2 SEM Micrographs of hydrothermally synthesized $Ag_2V_4O_{11}$ (SVO)

bigger than b or c, it is possible to obtain a reasonable approximation to the elongated rectangular particles shown in the SEM images of Fig. 2.

For a suspension in which ellipsoids are randomly arranged, the conductivity equation can be written as:

$$\sigma_c = \sigma_p + \frac{(\sigma_s - \sigma_p)(1 - f)}{1 + \frac{\rho}{3}\sum_{\alpha} \frac{\sigma_s - \sigma_p}{\sigma_p - \eta_\alpha \cdot \sigma_s}} \tag{1}$$

where f is the volume fraction of the suspended phase, η_α is the form factor which depends upon the ellipsoidal axial ratios, and σ_c, σ_p and σ_s are the conductivity of the composite, the particles and the solution, respectively. The

volume fraction of particles was estimated by:

$$f = \frac{(w/\rho)}{(\pi \cdot r^2 \cdot l)} \tag{2}$$

Here w is the weight of particles, ρ is their theoretical density and $(\pi \cdot r^2 \cdot l)$ is the volume of the PSC chamber. The form factors, η_α, used for this approximation were taken from table 1 of H. Fricke [21]. For $a/b=6$ and $b/c=2$ the form factors are $\eta_a=38.8$, $\eta_b=2.1$ and $\eta_c=0.53$.
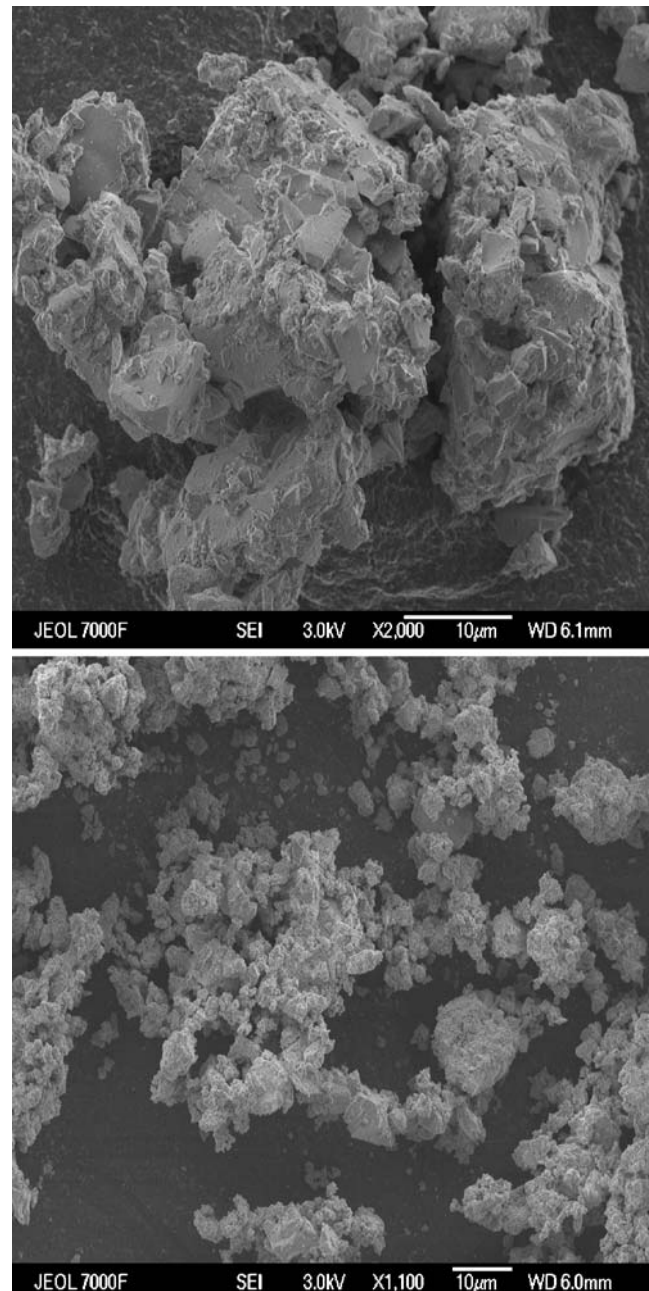

Fig. 3 SEM Micrograph of hydrothermally synthesized $Ag_4V_2O_6F_2$ (SVOF)

For the SVOF phase, SEM images show highly aggregated spherical-like aggregates with a broad range of sizes, and the effective medium found to give the best fit to the composite data is the Bruggeman asymmetric equation [5, 8, 22], given by:

$$\frac{K_c - K_p}{K_c^{1/3}\left(1 - K_p\right)} = (1 - f) \qquad (3)$$

where K_c is the conductivity ratio between the composite and the solution (σ_c/σ_s), K_p is the conductivity ratio between the particles and the solution (σ_p/σ_s), and f is the volume fraction of the suspended phase as calculated above in Eq. 2.

Although the conductivity of the particles can be directly calculated from a single datum using Eq. 1 or 3 (within the regime where $\sigma_p \sim \sigma_s$), the experimental error introduced by this individual calculation can lead to large errors in the calculation of σ_p. In order to address this error, several measurements were taken over a range of $AgNO_3$ solution conductivities, which is the basis of the PSC technique [8]. Figures 4 and 5 show the PSC plots for SVO and SVOF, respectively, where the conductivity of the composite is plotted versus the conductivity of the solution. The phase under study (SVO and SVOF) is represented with grey circles, the calculated fit is a dashed line and the plain solution is the thicker line. Individual error bars reflect uncertainty in measuring interelectrode spacing and in evaluating resistance from the corresponding cusp in the impedance plots (e.g., Fig. 1). An equivalent circuit model, in conjunction with the appropriate mixing laws discussed above, was used to simulate and fit the data (dashed lines)
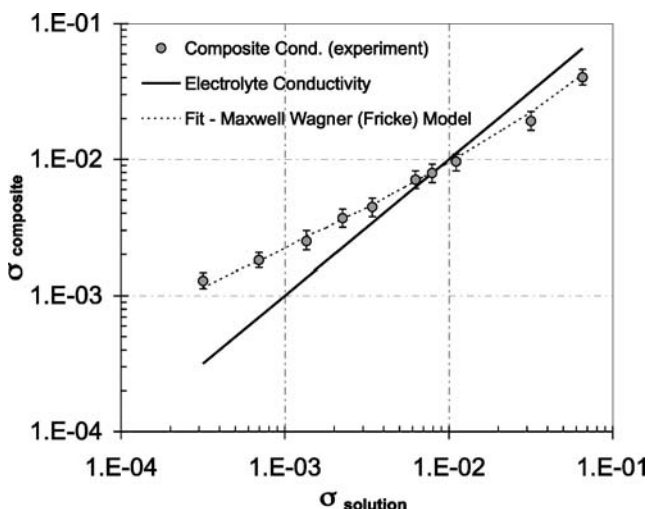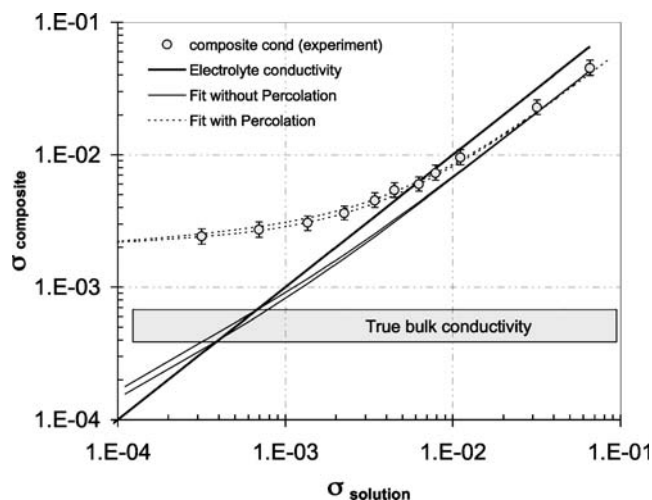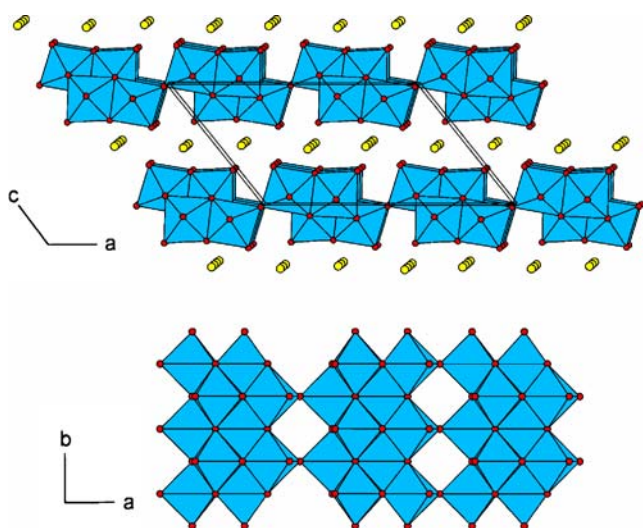

Fig. 5 Experimental results from SVOF (*grey circles*), simulated fit with percolation (*dashed line*), simulated fit without percolation (*solid line*) and plain solution (*thick solid line*). The conductivity of the particle was set to 0.0005 S/cm

in Figs. 4 and 5 [8, 14]. For the case of the SVO sample the crossover point between the fitted data and the plain solution gives the true bulk conductivity of the particles (0.0085 S/cm). The analysis is not as straightforward for the case of the SVOF sample. To fit the data we need to account for particle-to-particle conductivity (percolation), evident in the plateau at low solution conductivities in Fig. 5. The observed high deformability of the SVOF particles is in agreement with this hypothesis [23–27]. To account for the effect of percolation a parallel conduction path was added to the equivalent circuit model [8, 14]. This parallel conduction path presents a significantly lower resistance and at low electrolyte conductivities, currents prefer to flow through the particles than via the electrolytic media, explaining the origin of the constant composite conductivity at low solution conductivities. When the resistance of the percolation path is low, the crossover point becomes affected, and no longer corresponds to the particle conductivity. To retrieve the true bulk conductivity of the particles it is necessary to mathematically subtract the percolation contribution. When the percolation path is subtracted, the solid black lines are obtained; the crossover point in Fig. 5 is significantly lower. This intersection represents the true bulk conductivity of the SVOF particles.

To estimate uncertainty in the PSC analysis, the fitting procedure was repeated at the upper and lower limits of the experimental data as it can be seen in Fig. 5. The resulting uncertainties were 0.0085±0.0005 and 0.0005±0.00015 S/cm for the SVO and SVOF samples, respectively. The value for the SVO phase agrees well with the value reported by Onoda et al (~0.012 S/cm) on polycrystalline specimens of $Ag_2V_4O_{11}$ obtained by solid state reaction [28]. Their work involved four-point conductivity measurements on sintered
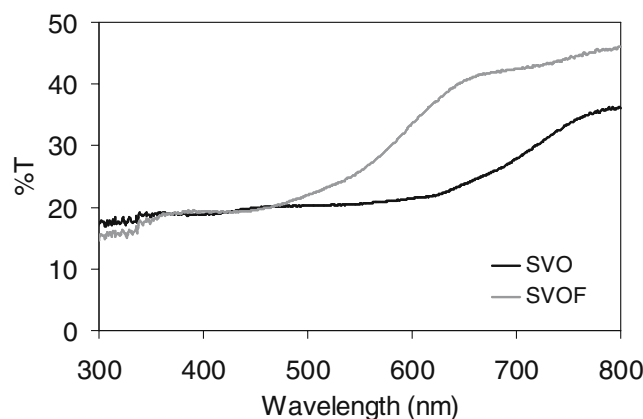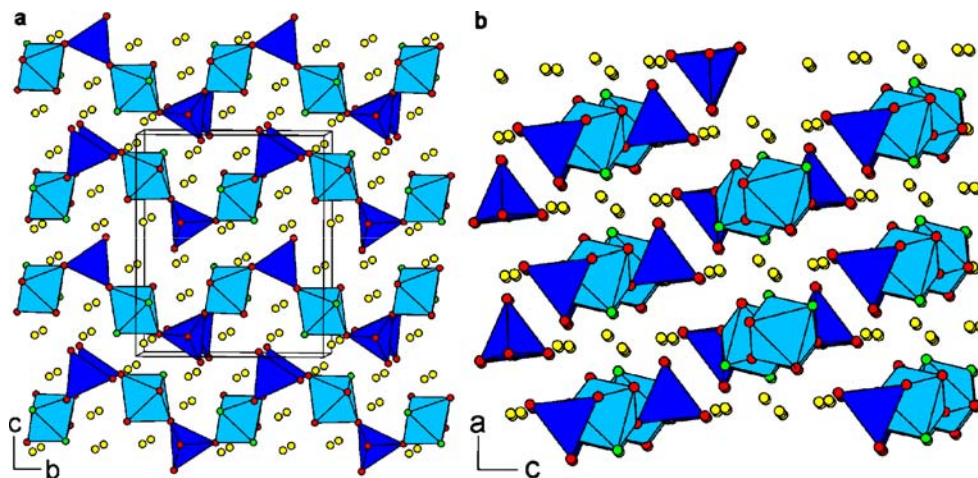

Fig. 4 Experimental results from SVO (*grey circles*), simulated (*dashed line*) and plain solution (*solid line*). The conductivity of the particle was set to 0.0085 S/cm

Fig. 6 Three dimensional packing diagram of $Ag_2V_4O_{11}$ (SVO) illustrating the layered nature of the structure. Silver atoms are represented in *yellow* and vanadium atoms in *blue*

Fig. 8 Diffuse reflectance of SVO, $Ag_2V_4O_{11}$, (*black line*) and SVOF, $Ag_4V_2O_6F_2$, (*grey line*)

pellets, which confirms the validity of the PSC technique. The conductivities obtained for the SVO and SVOF phases are in general agreement with values for the lithium storage cathodes currently used, such as the $LiMn_2O_4$ spinel ($\sim10^{-5}$ S/cm) and $LiCoO_2$ ($\sim10^{-3}$ S/cm) [27–30]. They also fall in the conductivity range of the more recently reported olivine-type materials (10^{-9} S/cm) and doped phospo-olivines (>0.001 S/cm) [7, 33]. It should be mentioned that for the case of both silver vanadates, the formation of silver metal during the discharge of the battery enhances the conductivity of the cathode.

The higher conductivity of the SVO phase compared to the SVOF phase is not surprising if we consider the structure of these two silver vanadates (see Figs. 6 and 7). Materials like SVO and SVOF, with layered structures, maintain their structural integrity during intercalation and deintercalation processes. SVO and SVOF both exhibit a type of layering that allows them to remain stable during

the discharge of the battery. The layers in SVO are comprised of either silver ions or distorted edge- and corner-sharing vanadium oxide octahedra (Fig. 6). The VO_6 octahedra are centered around either of two crystallographically distinct vanadium sites, V1 and V2. The octahedra around V1 share three edges and one corner and the octahedra around V2 share five edges, while each has one oxide ligand unshared with another vanadium oxide octahedron. The solitary silver position sits between the vanadium oxide layers and is coordinated to five oxide ligands, assuming a coordination sphere of 2.50 Å.

The extended network in SVOF is different from that of SVO in that the chains of vanadium-centered polyhedra in SVOF are not linked with adjacent chains; unlike in SVO where the chains of edge-sharing octahedra, observed along the *b*-axis, are linked to one another by corner-sharing connections. The chains in SVOF are constructed of alternating VO_4 tetrahedra and distorted VO_4F_2 octahedra, linked through bridging oxide ligands (Fig. 7). Sheets of undulating chains, which are absent of silver, comprise the two-dimensional structure necessary to maintain stability during intercalation. The four distinct silver positions rest

Fig. 7 Three dimensional packing diagram of $Ag_4V_2O_6F_2$ (SVOF) showing the alternating chains of vanadium oxide tetrahedral and vanadium oxide fluoride octahedra separated by silver ions

between the sheets of chains. The coordination around the silver ions ranges from 4- to 7-coordinate and consists of oxide and fluoride ligands.

The connectivity of the vanadium oxide layers of SVO versus the vanadium oxide chains of SVOF explains why SVO allows more facile electron flow. The proposed transport mechanism by Onoda et al. suggested that since vanadium ions are in a V^{4+}–V^{5+} mixed valence state, small polarons are formed owing to strong electron–phonon coupling [28]. PSC measurements at slightly different temperatures would be necessary to test this idea on SVOF.

Finally, diffuse reflectance spectra were collected to quantify the optical properties of these compounds. Figure 8 characterizes the optical properties of the uniaxially cold pressed silver vanadates samples. Transmission increases for the SVOF specimen as well as the optical gap. The values obtained for SVO and SVOF, which have distinct transition edges, are approximately 1.94 and 2.38 eV, respectively. Increased transmission is consistent with the drop in the number of carriers and consequently the lower conductivity found in the SVOF.

4 Conclusions

The silver vanadates, $Ag_4V_2O_6F_2$ and $Ag_2V_4O_{11}$, have been synthesized by a low temperature and low pressure hydrothermal technique. The electrical and optical properties of these materials have been examined, for the first time in the case of $Ag_4V_2O_6F_2$. Electrical conductivity was measured by the powder-solution-composite (PSC) method. $Ag_4V_2O_6F_2$ (SVOF) has several properties that make it a potentially useful primary lithium battery material. It has a higher silver-to-vanadium ratio than typical electrochemically active materials, while preserving critical connectivity in the vanadium oxide fluoride framework. However, the conductivity is lower than for the SVO phase, but still higher than other previously reported electrode materials [28–33]. SVOF has a larger band gap and lower visible light absorption concomitant with the lower conductivity.

References

1. J.-M. Tarascon, M. Armand, Nature **414**, 359 (2001)
2. C.L. Schmidt, P.M. Skarstad, J. Power Sources **97–98**, 742 (2001)
3. J. Drews, G. Fehrmann, R. Staub, R. Wolf, J. Power Sources **97–98**, 747 (2001)
4. C. Schmidt, G. Tam, E. Scott, J. Norton, K. Chen, J. Power Sources **119–121**, 979 (2003)
5. K.J. Takeuchi, A.C. Marschilok, S.M. Davis, R.A. Leising, E.S. Takeuchi, Coord. Chem. Rev. **219–221**, 283 (2001)
6. E.M. Sorensen, H.K. Izumi, J.T. Vaughey, C.L. Stern, K.R. Poeppelmeier, J. Am. Chem. Soc. **127**, 6347 (2005)
7. S.-Y. Chung, J.T. Bloking, Y.-M. Chiang, Nature **1**, 123 (2002)
8. B.J. Ingram, T. Mason, J. Electrochem. Soc. **150**, E396 (2003)
9. E.B. Segal, Chem. Heal. Saf. **7**, 18 (2000)
10. D. Peters, R.J. Miethchen, Fluor. Chem. **79**, 161 (1996)
11. J.C. Bertolini, J. Emerg. Med. **10**, 163 (1992)
12. W.T.A. Harrison, T.M. Nenoff, T.E. Gier, G.D. Stucky, Inorg. Chem. **32**, 2437 (1993)
13. B.A. Boukamp, *Equivalent Circuit for Windows* (University of Twente, The Netherlands, 2005)
14. L.Y. Woo, S. Wansom, T.O. Mason, J. Mater. Sci. **38**, 2265 (2003)
15. M. Campo, L.Y. Woo, T.O. Mason, E.J. Garboczi, J. Electroceramics **9**, 49 (2002)
16. R. Landauer, in *Electrical Transport and Optical Properties of inhomogeneous media*, ed. by J.C. Garland, D.B. Tanner, AIP Conf. Proc., vol 40 (American Institute of Physics, New York, 1978), p.2
17. R.E. Meredith, C.W. Tobias, in *Advances in Electrochemistry and Electrochemical Engineering*, vol. 2, ed. by C.W. Tobias (Interscience, New York, 1962), p. 15
18. J.F. Douglas, E.J. Garboczi, in *Advances in Chemical Physics*, vol. XCI, ed. by I. Prigogine, S. Rice (Wiley, New York, 1995), p. 85
19. E.J. Garboczi, J.F. Douglas, Phys. Rev. E **53**, 6169 (1996)
20. D.S. McLachlan, J.-H. Hwang, T.O. Mason, J. Electroceramics **5**, 37 (2000)
21. H. Fricke, J. Phys. Chem. **57**, 934 (1953)
22. H. Fricke, Phys. Rev. **24**, 575–587 (1924)
23. D. McLachlan, M. Blaszkiewicz, R. Newnhan, J. Am. Ceram. Soc. **73**, 2187 (1990)
24. J. Newman, J. Electrochem. Soc. **113**, 501 (1966)
25. B.J. Last, D.J. Thouless, Phys. Rev. Lett. **27**, 1719 (1971)
26. S. Kirkpatrick, Rev. Mod. Phys. **45**, 574 (1973)
27. D. Stauffer, *Introduction to Percolation Theory* (Taylor & Francis, London and Philadelphia, 1985)
28. M. Onoda, K. Kanbe, J. Phys., Condens. Matter **13**, 6675 (2001)
29. J. Molenda, A. Stoklosa, T. Bak, Solid State Ionics **36**, 53 (1989)
30. Y. Shimakawas, T. Numata, J. Tabuchi, J. Solid State Chem. **131**, 138 (1997)
31. H. Kawaia, M. Nagatab, H. Kageyamac, H. Tukamoto, Electrochim. Acta **45**, 315 (1999)
32. J. Molenda, Solid State Ionics **176**, 1687 (2005)
33. C. Delacourt, L. Laffont, R. Bouchet, C. Wurm, J.-B. Leriche, M. Morcrette, J.-M. Tarascon, C. Masquelier, J. Electrochem. Soc. **152**(5), A913–A921 (2005)